

Structural Studies of FIV and HIV-1 Proteases Complexed With an Efficient Inhibitor of FIV Protease

Mi Li,^{1,2} Garrett M. Morris,³ Taekyu Lee,⁴ Gary S. Laco,³ Chi-Huey Wong,⁴ Arthur J. Olson,³ John H. Elder,³ Alexander Wlodawer,¹ and Alla Gustchina^{1*}

¹Macromolecular Structure Laboratory, ABL-Basic Research Program, NCI-Frederick Cancer Research and Development Center, Frederick, Maryland

²Intramural Research Support Program, SAIC Frederick, NCI-Frederick Cancer Research and Development Center, Frederick, Maryland

³Department of Molecular Biology, The Scripps Research Institute, La Jolla, California

⁴Department of Chemistry and the Skaggs Institute for Chemical Biology, The Scripps Research Institute, La Jolla, California

ABSTRACT Three forms of feline immunodeficiency virus protease (FIV PR), the wild type (wt) and two single point mutants, V59I and Q99V, as well as human immunodeficiency virus type 1 protease (HIV-1 PR), were cocrystallized with the C2-symmetric inhibitor, TL-3. The mutants of FIV PR were designed to replace residues involved in enzyme-ligand interactions by the corresponding HIV-1 PR residues at the structurally equivalent position. TL-3 shows decreased (improved) inhibition constants with these FIV PR mutants relative to wt FIV PR. Despite similar modes of binding of the inhibitor to all PRs (from P3 to P3'), small differences are evident in the conformation of the Phe side chains of TL-3 at the P1 and P1' positions in the complexes with the mutated FIV PRs. The differences mimic the observed binding of TL-3 in HIV-1 PR and correlate with a significant improvement in the inhibition constants of TL-3 with the two mutant FIV PRs. Large differences between the HIV-1 and FIV PR complexes are evident in the binding modes of the carboxybenzyl groups of TL-3 at P4 and P4'. In HIV-1 PR:TL-3, these groups bind over the flap region, whereas in the FIV PR complexes, the rings are located along the major axis of the active site. A significant difference in the location of the flaps in this region of the HIV-1 and FIV PRs correlates with the observed conformational changes in the binding mode of the peptidomimetic inhibitor at the P4 and P4' positions. These findings provide a structural explanation of the observed K_i values for TL-3 with the different PRs and will further assist in the development of improved inhibitors. *Proteins* 2000;38:29–40. Published 2000 Wiley-Liss, Inc.†

Key words: enzymes; drug design; inhibition constant; structure comparison; AIDS

INTRODUCTION

In the last two decades diseases caused by retroviruses have emerged as major health problems and have led to extensive studies of these pathogens. Human immunodeficiency virus type 1 (HIV-1) infection eventually leads to

acquired immunodeficiency syndrome (AIDS), an often fatal disease. A similar disease has been observed in cats infected with feline immunodeficiency virus (FIV).^{1–4} Since the outbreak of the AIDS pandemic, intensive efforts have been made to develop antiretroviral therapies that target HIV-1.⁵ The identification of suitable animal models that mimic HIV-1 infection and the pathology seen in humans has been essential for testing anti-HIV-1 agents and vaccines in vivo.^{6–10} Although a number of anti-HIV-1 drugs specific for different viral components have been developed,^{11–13} the rapid emergence of drug resistance has become a major problem.^{14,15}

Retroviruses encode an aspartic protease (PR) responsible for the cleavage of Gag/Pol polyprotein precursors into individual functional proteins, thus making PR the target of an important class of anti-HIV-1 drugs.^{13,16} However, the emergence of resistant strains, in which the sequence of the viral PR is altered in a way that leads to the impairment of inhibition, has been very rapid.^{17–20} Despite its high structural homology to HIV-1 PR,²¹ FIV PR demonstrates poor binding of inhibitors currently in clinical use against HIV-1 PR. Differences in specificity are largely due to variation in the residues that are involved in direct enzyme-ligand interactions.²² Previous studies have shown that FIV PR contains, at stereochemically equivalent positions, amino acid residues that are identical to those found in drug-resistant forms of HIV-1 PR. The residues in wild-type (wt) FIV PR that match those of drug-resistant HIV-1 PRs include I37 (V32I), V59 (I50V), D105 (N88D), and M107 (L90M).^{19,22,23} (Note that residue numbers referring to HIV-1 PR are italicized throughout the text.) Thus, the development of a broad-based inhibitor that is efficacious against both HIV-1 and FIV PRs may

Grant sponsor: National Cancer Institute; Grant sponsor: National Institutes of Health; Grant numbers: P01GM48870 and R01AI40882.

G.S. Laco's present address is Department of Microbiology, University of Washington School of Medicine, Seattle, WA 98195.

The contents of this publication do not necessarily reflect the views or policies of the Department of Health and Human Services, nor does mention of trade names, commercial products, or organizations imply endorsement by the U.S. Government.

*Correspondence to: Dr. Alla Gustchina, ABL-Basic Research Program, NCI-Frederick Cancer Research and Development Center, Frederick, MD 21702. E-mail: alla@ncifcrf.gov

Received 10 May 1999; Accepted 17 August 1999

help in creating a drug that could inhibit drug-resistant mutants of HIV-1 PR.

Although even the most potent inhibitors of HIV-1 PR are usually very poor inhibitors of FIV PR, a few exceptions exist, including HBV-793²² and several compounds prepared at Lilly Research Laboratories.²¹ Kervinen et al.²⁴ carried out studies aimed at revealing the structural basis for the universal properties of these inhibitors. Until very recently, no efforts to improve the inhibitory properties of inhibitors against FIV PR had been reported. The first inhibitors specifically optimized to bind to FIV PR belong to a recently described series of C2-symmetric compounds containing (1*S*,2*R*,3*R*,4*S*)-1,4-diamino-1,4-dibenzyl-2,3-diol as P1-P1' units and different substituents at P3 and P3'.²⁵ However, the structural basis for the improved inhibition of FIV PR by these compounds has not yet been established. To investigate these effects in detail, we expressed two single mutants of FIV PR in which residues V59 and Q99 were mutated to the structural equivalents in HIV-1 PR, namely I50 and V82, respectively. Crystal structures of wt FIV PR and the mutants, FIV PR V59I and FIV PR Q99V, were determined at 1.9 Å resolution in complexes with the C2-symmetric inhibitor TL-3, which was specifically designed to inhibit FIV PR. In addition, the crystal structure of HIV-1 PR complexed with the same inhibitor was solved at 2.0 Å resolution. These structures, which revealed both similarities and differences in the binding mode of TL-3 to the variants of FIV PR and to HIV-1 PR, were analyzed in detail using computational approaches.

MATERIALS AND METHODS

Expression and Purification of PRs

Wild-type and mutant FIV PRs were expressed and purified as previously described,²⁵ using the FIV-34TF10 molecular clone²⁶ as a template for the polymerase chain reaction. HIV-1 PR corresponds to the HXB2 molecular clone of the virus²⁷ and was expressed and purified as described,²⁸ using the BH10 clone as a template.²⁹

Preparation of the TL-3 Inhibitor

The C2-symmetric diol inhibitor TL-3, which contains (1*S*,2*R*,3*R*,4*S*)-1,4-diamino-1,4-dibenzyl-2,3-diol as the P1-P1' units and Ala at P3/P3' positions, was synthesized and purified as previously described.²⁵ The inhibition constants for TL-3 against the FIV and HIV-1 PRs were determined as described.²⁵

Crystallization and Structure Solution

Before the crystallization trials, the FIV PRs were subjected to gel filtration on Superdex-75 (Pharmacia) in 50 mM sodium/potassium phosphate buffer, pH 7.4, containing 1 mM EDTA, 50 mM 2-mercaptoethanol, 150 mM NaCl, 5% glycerol, and 5% 2-propanol as previously described.²¹ Crystallization of the complexes of the native and mutant FIV PRs was carried out under similar conditions at 4°C, using the hanging-drop vapor diffusion method, as follows: 2.5 µL of FIV PR complexed with TL-3 at 7 mg/mL (1:4 molar ratio) in 50 mM imidazole-HCl, pH

7.0, containing 1 mM EDTA and 1 mM dithiothreitol (DTT) was mixed with an equal volume of 2 M ammonium sulfate, 0.1 M sodium acetate, pH 4.6 (Hampton Crystal Screen, solution #47). Crystals appeared within a few days and reached the size of 0.2 mm × 0.2 mm × 0.4 mm in 1 week. Crystallization solutions used for HIV-1 PR were 15% saturated ammonium sulfate, 85 mM sodium citrate/170 mM sodium phosphate, 6% 2-methyl-2,4-pentanediol (MPD), and 0.02% sodium azide, pH 6.2.

X-ray diffraction data were collected at room temperature, using either a DIP2020 image plate detector mounted on a Nonius FR-591 rotating anode generator operated at 45 kV and 100 mA, or a Bruker Hi-Star multiwire detector mounted on a Rigaku RU-200 rotating anode operated at 50 kV and 100 mA. Each data set was collected from a single crystal. Image plate data were processed using the program suite HKL2000,³⁰ while multiwire detector data were processed with the program SAINT. All FIV PR crystals were almost completely isomorphous in the space group P3₁21, with a monomer of the PR and half of the symmetric inhibitor TL-3 in the asymmetric unit (Table I). Hexagonal crystals of HIV-1 PR were unambiguously assigned to the space group P6₁22, rather than to the much more common quasi-isomorphous space group P6₁, since the scaling R factors were almost identical in both cases (Table I).

The initial refinement was carried out for all structures with the program XPLOR,³¹ according to a uniform protocol; the final refinement was done with the program SHELXL.³² For FIV PR, the structure deposited in the Protein Data Bank under the accession code 1fiv was used as a starting model,²¹ whereas the refinement of HIV-1 PR was based on the complex with the inhibitor LP-130.²⁴ The progress of the refinement was cross-validated by the R-free index,³³ which was calculated for about 10% of all collected reflections that were excluded from the refinement. The models were rebuilt with the program O.³⁴ The quality of the geometrical and stereochemical indices refinement was continuously monitored using the program PROCHECK.³⁵ Table I shows the refinement statistics and quality assessments.

Comparative Molecular Mechanics Analysis of the Crystal Structures

The crystal structures of the complexes of the inhibitor TL-3 with HIV-1 PR and FIV PR were analyzed using programs developed in the language Python^{36,37} and scripts written in the Biosym Command Language (BCL), with InsightII version 97.0.³⁸ After the symmetry-related subunit of the dimer was generated, the inhibitor in each of the four complexes was divided into eight separate residues, corresponding to the subsites P4 to P4' in the Schechter and Berger notation.³⁹ Hydrogen atoms were added to each complex and the AMBER force field was used to assign atom types and partial atomic charges to all the atoms. In accordance with the implementation of this force field in InsightII, the distance-dependent dielectric was set to 4*r*, while the 1,4 energy terms were scaled by a factor of 0.5. The distances between each hydrogen bond

TABLE I. Summary of Data Collection and Refinement Statistics for the Inhibitor TL-3 Complexed With HIV-1 PR and With the wt and Mutant FIV PRs

| | HIV-1 PR | wt FIV PR | FIV PR V59I | FIV PR Q99V |
|---------------------------------------|--------------------|--------------------|--------------------|--------------------|
| Space group | P6 ₁ 22 | P3 ₁ 21 | P3 ₁ 21 | P3 ₁ 21 |
| Resolution range for refinement (Å) | 10–2.0 | 10–1.9 | 10–1.9 | 10–1.9 |
| Unit cell parameters | | | | |
| $a = b$ (Å) | 63.202 | 50.745 | 50.75 | 50.76 |
| c (Å) | 83.464 | 73.458 | 73.30 | 73.36 |
| Number of unique reflections | 8,126 | 9,018 | 9,489 | 8,437 |
| Completeness (%) | 98.4 | 99.5 | 95.3 | 93.1 |
| R_{merge} (%) | 10.6 | 8.3 | 4.9 | 7.8 |
| Reflections used in refinement | 6,887 | 8,578 | 7,886 | 7,385 |
| Refinement | | | | |
| R-factor, all data (%) | 19.5 | 17.9 | 16.4 | 15.5 |
| Work R-factor, all data (%) | 18.6 | 17.6 | 16.7 | 15.7 |
| Free R-factor, all data (%) | 28.1 | 25.1 | 23.9 | 26.6 |
| Rms deviation from ideality (Å) | | | | |
| Bond distances | 0.006 | 0.005 | 0.006 | 0.006 |
| Angle distances | 0.023 | 0.021 | 0.023 | 0.024 |
| Planarity | 0.025 | 0.023 | 0.026 | 0.027 |
| Chirality | 0.039 | 0.035 | 0.042 | 0.041 |
| Temperature factors (Å ²) | | | | |
| All atoms | 34.53 | 31.63 | 24.90 | 25.39 |
| Protein main chain | 30.02 | 25.25 | 18.84 | 19.44 |
| Protein side chains | 38.57 | 35.19 | 28.22 | 27.76 |
| Inhibitor | 27.70 | 21.65 | 18.84 | 21.56 |
| Water | 50.80 | 48.95 | 43.67 | 45.65 |
| Number of water molecules | 36 | 60 | 79 | 77 |

donor and hydrogen bond acceptor oxygen were restrained using a flat-bottomed potential, to preferred minimum and maximum separations of 1.0 Å and 1.5 Å, respectively.

A short initial molecular mechanics minimization of 100 iterations, using the conjugate gradient method, was followed by 100 steps of equilibration at 300 K, and then by 1,000 steps of molecular dynamics. The duration of each time step was 1 fs, resulting in a total of 1.1 ps of molecular dynamics. Each simulation ended with 1,000 iterations of conjugate gradient energy minimization. Finally, the resulting structure of each complex was analyzed to determine the internal energy and the intermolecular interaction energies by residue and by atom.

Next, minimization was performed on the active-site residues, inhibitor, and water molecules. The active-site residues were defined as those PR residues that had some

or all of their atoms within 6 Å of the C β atoms of the inhibitor's backbone, or the O β (ether-like) atoms of the carboxybenzyl (Cbz) groups. These residues were as follows: HIV-1 PR: 8, 23, 25, 27–30, 32, 45–50, 53, 82, 84; wt FIV PR and FIV PR V59I: 13, 28, 30, 32–35, 37, 54–59, 98, 101; FIV PR Q99V: 13, 28, 30, 32–35, 37, 54–59, 98–99, 101. The AMBER force field was used, as before, and 1,000 iterations of conjugate gradients energy minimization were performed on each of the four complexes, followed by energy analysis by atom and by residue. The energy contributions from van der Waals and Coulombic terms were summarized for each of the eight residues in the TL-3 inhibitor.

RESULTS AND DISCUSSION

Comparison of TL-3 Complexed With wt FIV and HIV-1 PRs

Figure 1 shows the superimposed ribbon structures of wt FIV and HIV-1 PRs, complexed with the inhibitor TL-3. The PRs of FIV and HIV-1 are 116 and 99 amino acids in length, respectively. Five of the additional amino acids in FIV PR reside at the N-terminus, while the remaining 12 occupy three external loops. Despite the remarkable similarity of the central parts of the active site regions in the complexes, significant differences are evident in the conformation of TL-3 beyond P3 and P3'. In all three complexes of FIV PRs, the Cbz groups are located along the major axis of the inhibitor's backbone, whereas in HIV-1 PR, they extend over the flaps (Fig. 1). Significant conformational changes can also be seen along the adjacent parts of the inhibitor's main chain. The peptide bond between the Cbz group at P4/P4' and Ala at P3/P3' in the inhibitor bound to HIV-1 PR is flipped $\sim 180^\circ$ as compared to the orientation in the TL-3:FIV PR complexes (Fig. 2). The latter conformation is the one normally adopted in the complexes of retroviral PRs with peptidomimetic inhibitors. In the TL-3:FIV PR complexes, the CO and NH groups of this peptide form hydrogen bonds with the NH of Ile57 and O $\delta 2$ of Asp34, respectively, having lengths of 2.8 Å and 3.0 Å. The orientation of the Asp34 side chain is also stabilized by the formation of two more hydrogen bonds with Arg13' (2.8 Å) and Arg104 (2.6 Å). This orientation and the interactions with the two Arg residues are also seen in the TL-3:HIV-1 PR complex, whereas the O $\delta 2$ atom of Asp29 is hydrogen bonded to the carbonyl oxygen (rather than to the NH group) of the flipped peptide bond of the inhibitor. Two water molecules not seen in the FIV PR complexes are located within the TL-3:HIV-1 PR complex, coordinated between Asp29 and Lys45 (Fig. 2a). One of these waters is located within short hydrogen bonding distance (2.73 Å) to the O $\delta 2$ atom of Asp34 and a longer distance (3.10 Å) to the carbonyl oxygen of the flipped peptide bond of the inhibitor. These interactions may facilitate proper positioning of the hydrogens in this complex network.

Recently, Kervinen et al.²⁴ compared the structures of the complexes of HIV-1, FIV, and equine infectious anemia virus (EIAV) PRs with a universal inhibitor, LP-130. This hexapeptide-mimicking inhibitor binds in nearly identical conformations in all three enzymes, unlike TL-3 in the

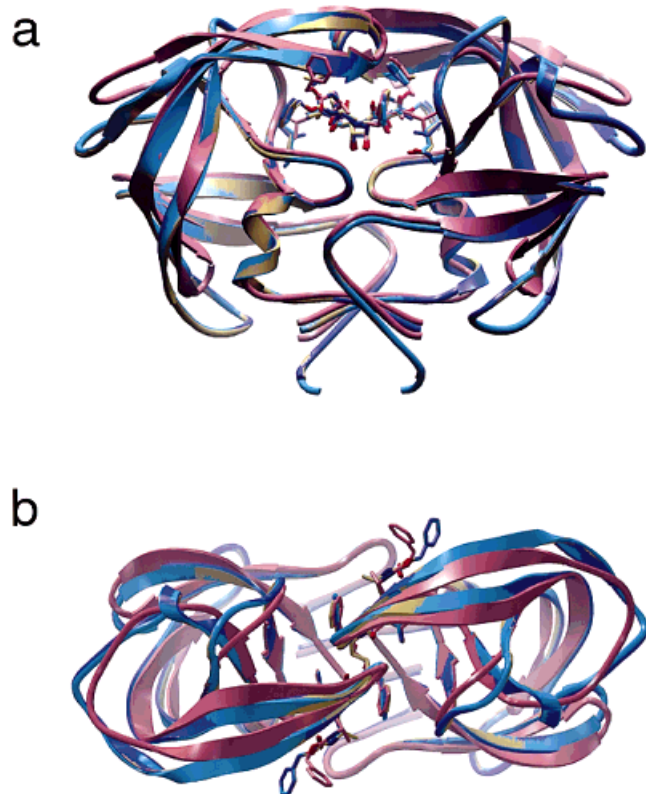


Fig. 1. Comparison of the complexes of TL-3 with wt FIV PR (blue), FIV PR V59I (yellow), FIV PR Q99V (purple), and wt HIV-1 PR (pink). The backbones of the PRs are shown as ribbons, whereas the inhibitors are shown as stick models. The residues that are mutated can also be seen. The complexes are shown in two orthogonal projections. **a**: the “front” view, looking down the active sites; **b**: the “flap” view, looking down on the flaps and the active site.

present study when bound to FIV and HIV-1 PRs. It should be emphasized that these differences are observed only at the ends of the inhibitor, beyond the P3/P3' positions. Figure 3 shows the superposition of the structures of two HIV-1 PR complexes, one with TL-3 and the other with U-85548e,⁴⁰ as well as FIV PR complexed with TL-3. There is an important difference in the position of the flaps in FIV PR and HIV-1 PR: in FIV PR, the flaps are closer to the active-site loops and to the ligand in the vicinity of P4/P4' sites than in HIV-1 PR. The distance between structurally equivalent C α atoms in the flaps of both enzymes is about 0.7 Å at Ile57/Gly48, and increases to about 2 Å at Gln54/Lys45. It is quite likely that because of this difference, substrates and ligands in FIV PR can extend along the active site groove for at least one more peptide bond beyond P3/P3', while still maintaining interactions with the enzyme on both sides of the active site. This structural result is in agreement with the previously reported requirement of FIV PR for longer peptide substrates than those required by HIV-1 PR.⁴¹ The orientation of the TL-3 Cbz group complexed with HIV-1 PR corresponds to the direction of the peptide bond between Ser at P4 and Val at P5 in the U-85548e inhibitor/HIV-1 PR

TABLE II. Inhibition of wt and Mutant FIV and HIV-1 PRs by the Inhibitor TL-3[†]

| Protease | K _i (nM) ^{1,2} | IC ₅₀ (nM) |
|--------------------------|---------------------------------------|--------------------------|
| wt FIV PR ³ | 41 ± 7 | nd ⁸ |
| FIV PR V59I ⁴ | 22 ± 5 | nd |
| FIV PR Q99V ⁵ | 8.3 ± 1.3 | nd |
| wt HIV-1 | 1.5 ± 0.3 | 3.8 |
| HIV-1 G48V ⁶ | nd | 20.5 |
| HIV-1 V82F ⁶ | nd | 14.9 |
| HIV-1 B273 ⁷ | nd | 31 |

[†]K_i and IC₅₀ values were determined twice.

¹Data for wt FIV PR and its mutants were obtained at 37°C in 0.1 M NaH₂PO₄, 0.1 M sodium citrate, 0.2 M NaCl, 0.1 mM DTT, 5% glycerol, and 5% DMSO in volume, pH 5.25.

²Data for HIV-1 PR and its mutants were obtained at 37°C in 0.1M Mes, 5% glycerol, and 5% DMSO in volume, pH 5.25.

³Wild-type PR of FIV (FIV-34TF10) or HIV-1 (HIV_{sf2}).

⁴V59I, FIV PR equivalent of position 150 in HIV-1 PR.

⁵Q99V, FIV PR equivalent of position V82 of HIV-1 PR.

⁶G48V and V82F, changes associated with drug-resistance development in HIV-1 PR.

⁷B273 (HIV-1 PR from a patient resistant to Saquinavir and Indinavir) contains the drug-resistance mutations I84V and L90M, as well as six other amino acid changes relative to wt HIV_{sf2} PR.

⁸Not determined.

complex (Fig. 3). The distance between the flaps and the active-site loops in HIV-1 PR is too large to stabilize the interactions of the inhibitor with the residues on both sides of the active site in this region. The interactions with the flap residues appear to be dominant, and the shift in the position of the ligand beyond P4/P4' in HIV-1 PR towards the flap is evident in the structures of HIV-1 PR complexed with either TL-3 or with U-85548e.

Comparison of the Inhibitor Interactions With the Wild Type and Mutant FIV PRs

Two single point mutants of FIV PR, V59I and Q99V, were prepared in order to introduce the residues from the structurally equivalent positions in HIV-1 PR. We expected that these mutations would alter the specificity of FIV PR and make the enzyme more similar to HIV-1 PR, consistent with the observed improvement of K_i values relative to that of wt FIV PR (Table II). Both FIV PR mutations improved the inhibition constant of TL-3 with respect to that of wt FIV PR, although the inhibition of HIV-1 PR remained strongest.

As expected, the mutations did not cause any significant modification of the enzyme structure. The root-mean-square (rms) deviation between the C α coordinates of one subunit of the dimer of the Q99V mutant and the wt FIV PR is 0.14 Å (with a maximum deviation of 0.39 Å), whereas that for the V59I mutant is 0.14 Å (0.38 Å). In

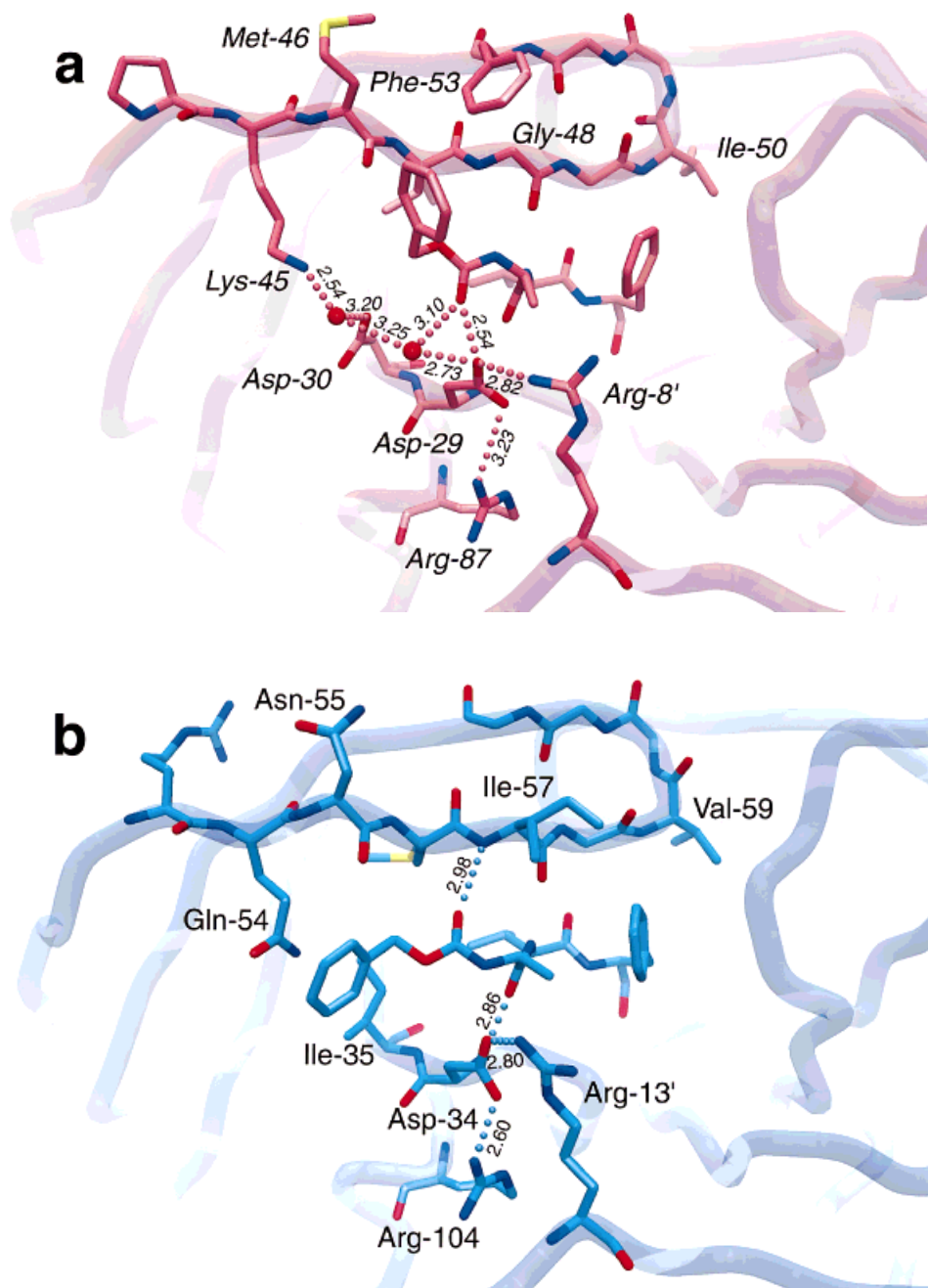


Fig. 2. TL-3 complexes of HIV-1 and FIV PRs near the S4 binding pocket. **a:** HIV-1 PR (pink); **b:** wt FIV PR (blue). Two different conformations of the Cbz groups and the adjacent peptide bonds are clearly visible. Two water molecules that are bound within the S4/S4' subsites of

TL-3:HIV-1 PR complex but are absent in the S4/S4' subsites of inhibitor complexes with wt and mutant FIV PRs are shown as pink spheres. The hydrogen bonds are shown by dotted lines, with the numbers corresponding to distances in angstroms between the interacting atom pairs.

contrast, the rms deviation between the native forms of FIV PR and HIV-1 PR is 1.10 Å for the 91 C α pairs that could be directly superimposed. The differences between the backbone structures of wt and mutant FIV PRs are well within the range of uncertainty expected for structures at this resolution, so their overall differences cannot be considered significant.

Figure 4 shows the superposition of the crystal structures of the inhibitor complexes of the wt and mutant FIV

PRs. Only half of the inhibitor molecule is shown, since the other half is generated by crystallographic twofold symmetry. The conformations of TL-3 in the three complexes are almost identical, with the exception of the aromatic ring of Phe at P1/P1'. In the inhibitor complexes of both mutants, the aromatic ring is shifted toward the flap, thus resembling the complex with HIV-1 PR. These conformational changes are mostly due to small rotations around the C α -C β and C β -C γ bonds of the Phe side chain. When

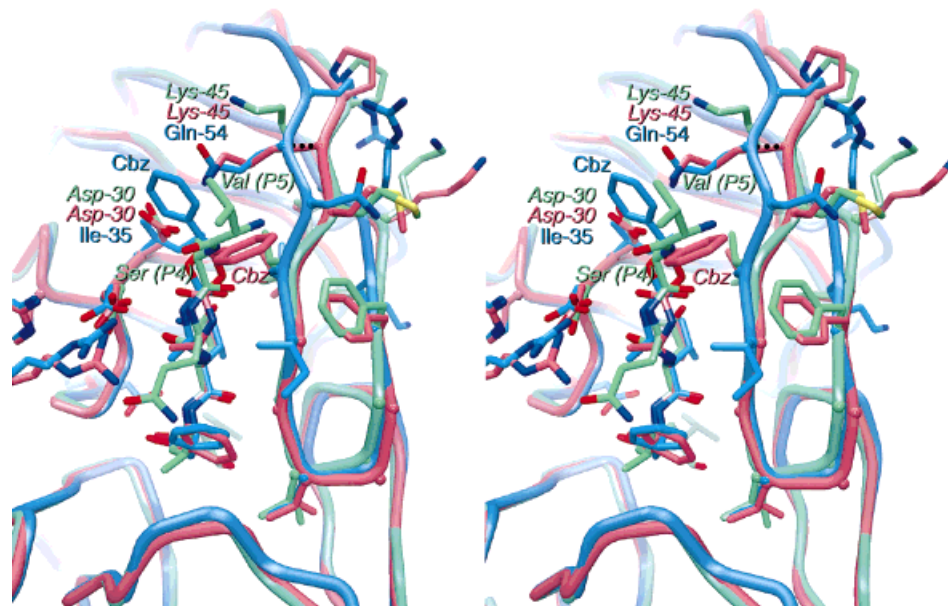


Fig. 3. Stereoview of the superimposed structures of wt FIV PR (blue) and HIV-1 PR (pink) complexed with TL-3, and the structure of HIV-1 PR complexed with U85548e40 (green). The Cbz group in TL-3 that is bound to HIV-1 PR follows the orientation of the P4-P5 peptide bond in

U-85548e. The shift in the main chain of the flaps in the FIV and HIV-1 PRs in this region can be clearly seen. The black dots (upper right) indicate the 2 Å shift in the flap C α atoms of FIV PR, versus HIV-1 PR, when bound to TL-3.

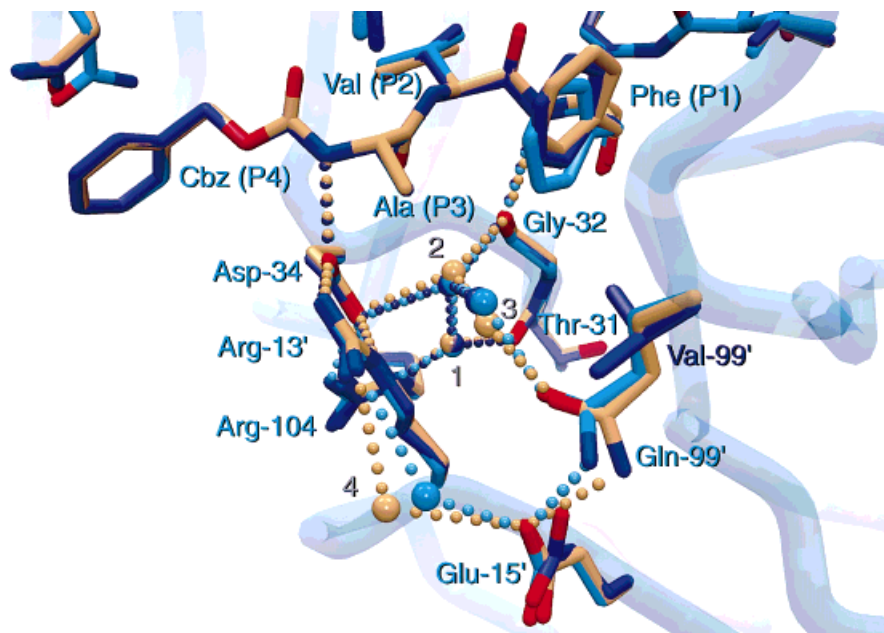


Fig. 4. Superposition of the crystal structures of wt FIV PR (blue) and its two mutants, V59I (yellow) and Q99V (purple), complexed with TL-3, near the S1 binding site. Water molecules are shown as spheres, whereas hydrogen bonds are shown as dotted lines.

superimposed directly, the inhibitors deviate by 0.23 Å between wt FIV PR and the Q99V mutant, whereas the deviation is 0.35 Å between wt FIV PR and the V59I mutant. Four water molecules are shown in Figure 4. Water molecules 1 and 2 bridge the carbonyl oxygens of

Thr31 and Gly32 in the FIV PR structures via three consecutive hydrogen bonds. Similar interactions were found in the structures of various retroviral proteases.²² Water molecules 3 and 4 maintain the interactions between residues Glu15', Arg13', and Gln99 of wt FIV PR,

Fig. 5. Distribution of the atomic temperature factors in the structures of three FIV PRs (wt and two mutants) complexed with TL-3. The atoms of the PRs are color coded by the values of individual B factors, with blue corresponding to low values and red corresponding to high values. **a:** wt FIV PR; **b:** FIV PR Q99V; **c:** FIV PR V59I.

and the Phe side chain of the inhibitor. In the Q99V mutant, one of these water molecules is not present and the Phe side chain at P1/P1' is shifted toward the more hydrophobic area near the flap. Although Q99 is present in the structure of the V59I mutant and the water structure is preserved, the Phe ring is nevertheless moved in the direction of the flap into the more hydrophobic environment (Fig. 4). These shifts are not very large, ranging between 0.29 Å and 0.41 Å for the C γ atoms of the Phe rings; however, the combined effects of many small structural changes have a significant effect on the overall inhibition constant (Table II) and on the overall temperature factors. As shown in Table I, the average B-factor is consistently lower for the main chain, side chains, and all atoms in both mutants. This phenomenon is illustrated in Figure 5, which shows the decrease in the temperature factors throughout both mutants, including the surface residues, despite the fact that the differences in the structures are localized primarily around the mutation sites.

The Interface between the Flexible and Rigid Parts of the PR Active Sites

The interface between the flap and loop 93–98 in FIV PR shows a pattern of interactions that is not present in HIV-1 PR, since several differences in residue types are evident at this region (Fig. 6). These differences change the pattern of interactions between three important secondary structural elements—namely, the flap region, loop 93–98 (79–

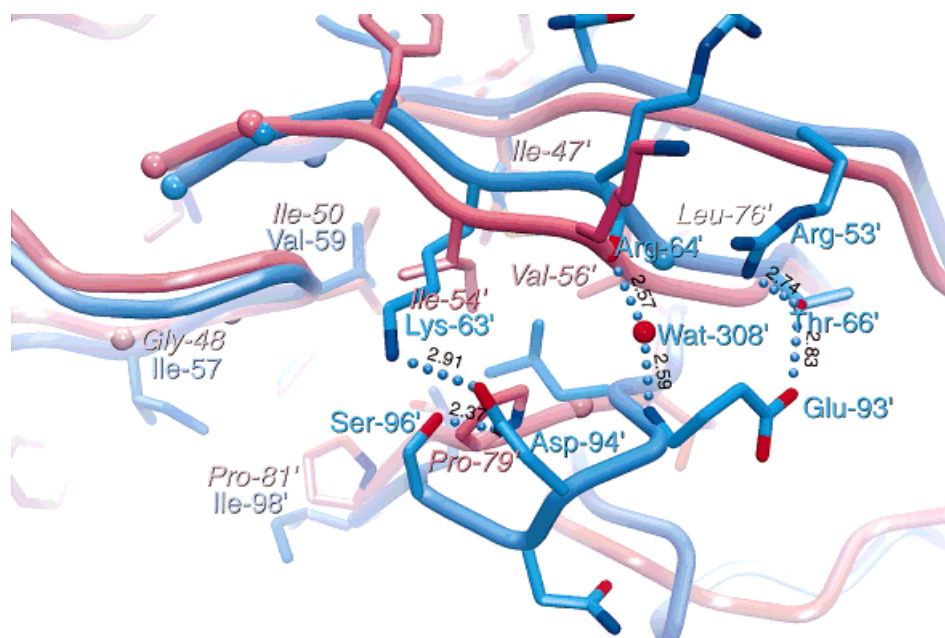
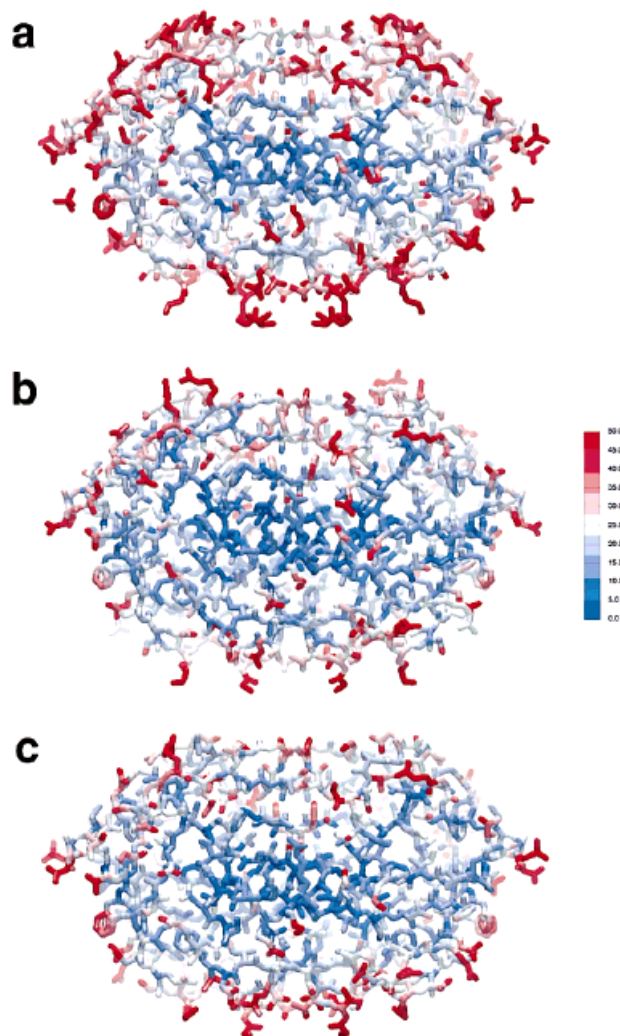


Fig. 6. Comparison of the interface between the flap region and loop 93–98 (76–81) in wt FIV PR (blue) and HIV-1 PR (pink).

82), and the active-site loop 28–37 (23–32), which contains the catalytic residue Asp30 (*Asp25*). In HIV-1 PR, these interactions are mostly hydrophobic (Fig. 6) and involve flap residues *Ile47*, *Ile54*, *Val56*, *Leu76*, and *I50'*, as well as two Pro residues (*79* and *81*) in loop 79–82. In FIV PR, Lys63 is found in place of *Ile54*, Gly65 for *Val56*, and *Ile57* for *Gly48*. In the loop region, Ser96 and *Ile98* substitute for *Pro79* and *Pro81*; furthermore, three additional residues (93–95) are inserted in FIV PR, changing the conformation of this loop. These latter three residues do not have equivalents in the structures of other known retroviral PRs. Two of these residues interact with flap residues: Glu93 forms a hydrogen bond with Thr66 (Fig. 6), whereas Asp94 forms a hydrogen bond with Ser96 (*Pro79*) and appears to be favorably oriented to form a salt bridge with Lys63 (*Ile54*) when the flaps are in a closed conformation. The position of Thr66 is stabilized by an additional hydrogen bond with Arg53. The β -sheet formed between the flap and loop 93–98 in all of the FIV PR structures is one peptide longer than in the HIV-1 PR structure. The backbone carbonyl oxygen of Arg64' is hydrogen-bonded to the amide nitrogen of Glu93' via Wat308 (Fig. 6). This water molecule is conserved in all three complexes of FIV PR. Therefore, the interactions with the flap in this region of FIV PR are charged and hydrophilic, unlike their hydrophobic counterparts in HIV-1 PR. In addition, in FIV PR extra hydrophobic interactions between the same loop and the flap from the second monomer are formed by the residues *Ile98* and *Ile57'* (*Pro81* and *Gly48'* respectively), favoring a closed conformation of the flaps. The presence of *Ile35*, *Leu92*, and *Leu97* in FIV PR (equivalent to *Asp30*, *Gly78*, and *Thr80* in HIV-1 PR) contributes to the continuous hydrophobic core and stabilizes the interactions with the more rigid part of the molecule, which includes the active-site loops.

Comparative Molecular Mechanics Analysis of the Crystal Structures

Figure 7 shows the results of the per-residue AMBER energy analysis of the active site-minimized structures, indicating the van der Waals (vdW) and Coulombic energy contributions to the nonbonded intermolecular interaction energy between the active site and the TL-3 inhibitor. There are several important features to note: (1) TL-3 has stronger vdW interactions in the subsites of the HIV-1 PR complex than in the FIV PR complexes, except for P2' (Fig. 7a). (2) Conversely, TL-3 has stronger Coulombic interactions in the subsites of the FIV PR complexes than in the HIV-1 PR complex, except for P1 and P2' (Fig. 7b). These differences reflect the fact that the interactions of TL-3 with HIV-1 PR are more hydrophobic, while in FIV PR they have a more hydrophilic character. The asymmetry in the interactions in the TL-3:HIV-1 PR complex is primarily due to the disordered Phe53 residue, which in the A chain angles towards the P4 carboxybenzyl group (Cbz), and in the B chain angles up and away from the P4' Cbz. (3) The Coulombic energies for TL-3 at P4/P4' and P3/P3' subsites in all three FIV PR complexes are all lower than in the HIV-1 PR complex. This is partly due to the plane of the

peptide group that links the P4/P4' and P3/P3' moieties being flipped by $\sim 180^\circ$. Both the CO and NH groups of this peptide bond are involved in the formation of two hydrogen bonds in all three FIV PR complexes, but only one hydrogen bond exists in the HIV-1 PR complex. By inspecting the per-atom energy (data not shown), we found that this energy difference is due primarily to the formation of a hydrogen bond that is present only in the FIV PR complexes between the backbone NH of I57 to the Cbz-carbonyl oxygen atom. A similar situation pertains to the P3/P3' moieties: The Ala backbone carbonyl and amide NH groups of TL-3 have greater vdW and Coulombic stabilization in the FIV PR complexes than in the HIV PR complex, due to an extra hydrogen bond between the Ala-NH and the proximal O δ of Asp34 in TL-3:FIV PR. Both of these improvements in the calculated binding enthalpy at P4/P4' and P3/P3' are due to the flipping of the intervening peptide bond in TL-3:HIV PR relative to the TL-3:FIV PR complexes. (4) The terminal Cbz groups and the Ala residues at P3/P3' in TL-3:HIV-1 PR have more negative (i.e., better) vdW energies than those in the FIV PR complexes. This result suggests that the decreased (i.e., improved) inhibition constant of TL-3 with HIV-1 PR relative to that with FIV PR could be due to better packing of the Cbz groups against the flaps of HIV-1 PR.

The segment comprising residues Gly58, Val59, Gly60, Gly61 and Gly62 has two orientations in wt FIV PR. In addition, side chains *Ile37* and *Ile108* in FIV PR V59I, and *Ile57* and *Ile108* in the FIV PR Q99V are also disordered. In HIV-1 PR, however, only one residue in each subunit of the dimer, *Phe53*, is disordered. Most of these disordered side chains are located near the active site, in the flap region, and at the S1/S1': and S3/S3' subsites. These minor differences in interaction between the residues of TL-3 and the slightly different subunits of various PR dimers give rise to the subtle differences that can be seen in the C2-symmetry-related components of the nonbonded energy.

Difference Distance Matrices

Figure 8 shows the results of subtracting the distance matrices for pairs of wt and mutant FIV PRs. The distance matrices represent the distances between all pairs of C α atoms in both chains of the PR (A5–A116 and B5–B116) and in the chain of the inhibitor (I1–I8), which results in 232 residues along each axis. The residue numbers are shown across (left to right) and down the square matrices. The “difference distance matrix” (i.e., the difference between the distance matrices of two PRs), is calculated for three comparisons: wt to V59I, wt to Q99V, and V59I to Q99V. The results are color-coded as follows: Negative values are pink, zero values are white, and positive values are blue. Thus, to compare the distance between residue *i* and residue *j* in one PR, *A*, with that of the same pair (*i,j*) in another PR, *B*, we simply calculate the change in distance, $d((i,j), A) - d((i,j), B)$. If this value is negative, then $d(A) < d(B)$, which indicates that these residues move further apart going from *A* to *B*; therefore, this residue pair appears pink in the matrix. If the distances are the same,

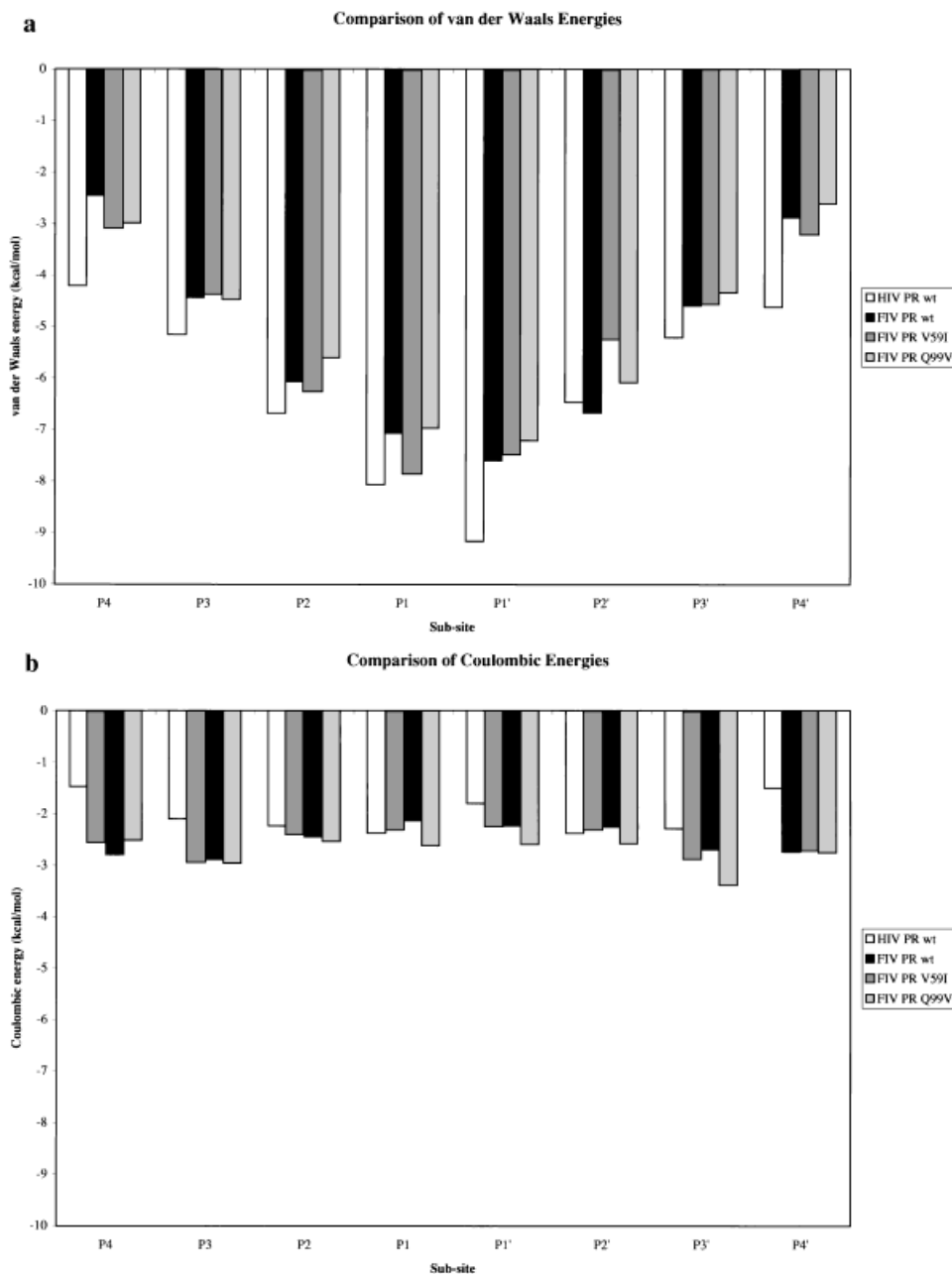


Fig. 7. Variation in van der Waals and Coulombic energy components. **a:** Variation of the van der Waals component of the AMBER nonbonded intermolecular interaction energies by subsite, for wt HIV-1, wt FIV, FIV V59I and FIV Q99V PRs. Note that the energies at the P4/P4' and P3/P3'

subsites in HIV PR are lower, i.e., more stable, than in any of the FIV PRs. **b:** Variation of the Coulombic component of the AMBER nonbonded intermolecular interaction energies by subsite, for wt HIV-1, wt FIV, FIV V59I, and FIV Q99V PRs.

the difference is zero, and this residue pair appears white. Finally, if the difference in distances is positive, then $d(A) > d(B)$; these residues move closer together from A to B, and this pair appears blue in the matrix.

wt FIV PR – FIV PR V59I

Figure 8a shows the difference distance matrix which results from subtracting the distance matrix for the mutant FIV PR V59I from the distance matrix for wt FIV PR. The vertical blue bands pointed out in the figure (see

“tightening of the flaps”) indicate that the first β strand of the flaps (residues A50–A60 and B50–B60) moves closer to the inhibitor. Note also that the second β strand of the flap in chain B also moves closer to the inhibitor, as indicated by the vertical blue band, around B60–B70, in the lower half of the matrix. The K_i values for TL-3 decrease from 41 nM for wt FIV PR to 22 nM for the V59I mutant, and the difference distance matrix indicates that this is partly due to the subtle but extensive tightening of the flaps around the inhibitor and consequently the active site.

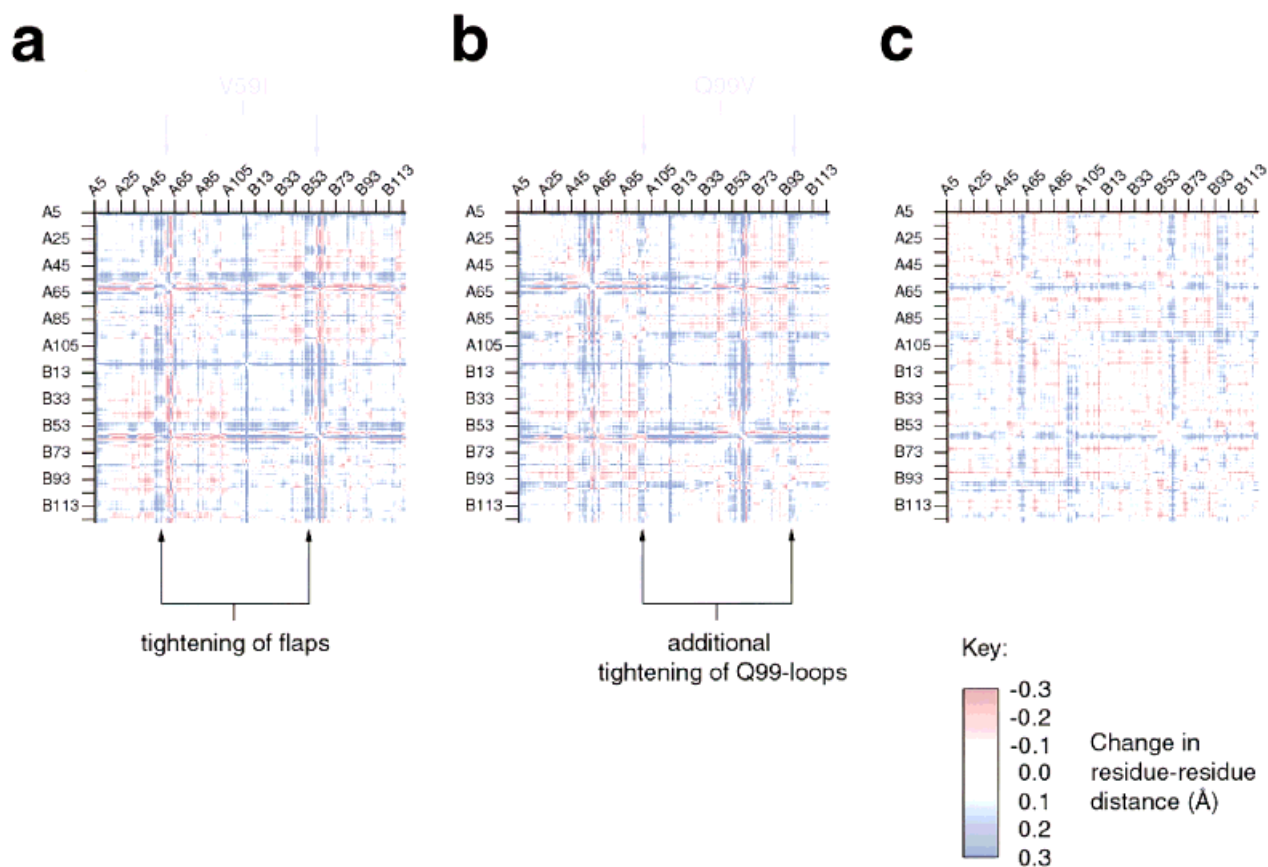


Fig. 8. Difference distance matrices comparing the structures of the three TL-3:FIV PR complexes. For definitions, see text. **a:** wt FIV PR and FIV PR V59I; **b:** wt FIV PR and FIV PR Q99V; **c:** FIV PR V59I and FIV PR Q99V. Note the added stabilization in both the V59I and Q99V mutants relative to wt FIV PR due to the tightening of the flaps (vertical blue bands

indicated in panel a) and the increased stabilization in FIV PR Q99V due to the tightening of the mutation-bearing loops (extra vertical blue bands indicated in panel b). The subtle differences between the two subunits of the V59I and Q99V dimers, thanks to side chain disorder, can be seen in the asymmetric pattern in panel c.

wt FIV PR – FIV PR Q99V

The pattern of changes in distances between wt FIV PR and the Q99V mutant is quite similar to that of wt FIV PR and the V59I mutant, with an important exception: there is an additional region in both FIV PR Q99V chains (residues 95 to 105) that also tightens against most of the rest of the PR and the inhibitor (Fig. 8b). This region is close to the inhibitor—specifically, near the P1/P1' and P3/P3' subsites. These additional regions of the PR that move closer together may well account for the increased stabilization observed in the more tightly bound TL-3:Q99V complex ($K_i = 8$ nM) compared with that of the TL-3:V59I complex ($K_i = 22$ nM).

FIV PR V59I—FIV PR Q99V

The comparison of the two mutants (Fig. 8c) highlights the fact that the flaps (around A60 and B60) and the loop region containing the Q99V mutation close in and tighten the binding of the TL-3 inhibitor. This loop also tends to move closer to the opposite chain, i.e., the loop from A93 to A103 moves closer to the inhibitor and the B subunit of the PR, while the region from B93 to B103 moved closer to the

inhibitor and the A subunit. This pattern appears to stabilize the Q99V dimer relative to the V59I dimer.

CONCLUSIONS

TL-3, the first inhibitor designed specifically for FIV PR, binds even more tightly to HIV-1 PR, and to mutants of FIV PR with amino acid replacements that emulate HIV-1 PR. Importantly, recent results show that the C2-symmetric TL-3 is also efficacious against the drug-resistant mutants of HIV-1 PR that are commonly found in clinical isolates. In this study, we compared the crystal structures of TL-3 complexed with the wild type and mutant forms of FIV PR, as well as with HIV-1 PR. We found substantial differences between the HIV-1 and FIV PR complexes in the binding mode of the inhibitor Cbz groups and the adjacent peptide bonds within the S4-S5/S4'-S5' binding pockets. These differences correlate with a significant shift in the positions of the flaps in this region of the active sites of the HIV-1 and FIV PRs. We propose that during the early stages of substrate binding, a single β -sheet might be formed between the substrate's main chain and the flap. A comparison of the structural data presented here and

published previously,⁴¹ indicates that this β -sheet may be longer in FIV PR than in HIV PR and involves residues in the substrate beyond the P4/P4'. This hypothesis is in good agreement with the previously shown requirement for a longer substrate by FIV PR, although experimental confirmation is still needed.

In addition, conformational differences are evident in the orientation of the P1 and P1'; Phe rings of TL-3 in the FIV and HIV-1 PR complexes, with the position of the Phe side chains in both mutant FIV PR complexes being more similar to those in the HIV-1 PR complex. This shift of the Phe residues toward the flap region increases the interactions between the flexible and more rigid parts of the active site via the ligand. These data emphasize the importance of the interactions between the more flexible parts of the active site—namely, the flaps, and the more rigid parts of the molecule. Moreover, the data demonstrate that the interactions between the flap and the active-site loop are quite distinct in the FIV and HIV-1 PR complexes, with mostly polar interactions in TL-3:FIV PR versus predominantly hydrophobic interactions in TL-3:HIV-1 PR.

Although both mutants of FIV PR show small shifts of the Phe rings of TL-3 at the P1/P1' positions toward the flap, thus resembling TL-3:HIV-1 PR, they still resemble the conformation of TL-3:wt FIV PR at P4/P4'. However, the extent of this shift at P1/P1' is not consistent with the changes in the inhibition constants of the two mutant FIV PRs. The V59I mutant, which has a twofold improved K_i with TL-3, shows a slightly larger shift toward the flap than does the Q99V mutant, which shows an approximately fivefold improvement in K_i with the inhibitor. One possible explanation for the improved K_i of TL-3 with Q99V relative to V59I may be the added stabilization revealed by the difference distance matrices. These matrices compare all the residues with one another, and thus give a more global picture of the structural changes. Both the flaps and the loops bearing the Q99V mutation tighten around the inhibitor compared with their counterparts in the wild-type enzyme; whereas only the flaps, which carry the mutation, tighten in the V59I mutant.

All four crystal structures reveal the presence of two "structural" waters in each subunit of the dimer (waters 1 and 2, shown in Figure 4 for FIV PRs). It was shown that the presence of these water molecules in the active sites of various retroviral PR:inhibitor complexes and the interactions they maintain are influenced by the size of the residue at P3/P3' in the ligand.²² Therefore, these water molecules may represent an additional target for drug design, not unlike Wat301, which is incorporated in the inhibitors containing cyclic urea.⁴² This knowledge could be exploited in the design of PR inhibitors with improved inhibition constants and good resistance-evading properties. An analysis of the crystal structures of these TL-3:PR complexes suggests that Ser at P3/P3' could hydrogen bond with one of these water molecules in each subunit. A residue even longer than Ser that contains a side chain hydroxyl might displace one of these waters. The enthalpy of binding should be unaffected if the hydroxyl is able to

form the same hydrogen bonds as the waters, but the entropic gain from liberating the two ordered water molecules (one in each subunit of the dimer) should improve the K_i .

ACKNOWLEDGMENTS

A.G. and A.W. would like to express gratitude to Professor Sir Tom Blundell for accepting them as Visiting Scientists in the Department of Biochemistry, University of Cambridge, where this paper was written. A.W. would also like to thank the Master and Fellows of the Sidney Sussex College for a Visiting Fellowship. This work was supported in part by the National Cancer Institute, DHHS, under contract with ABL and in part by NIH grants P01GM48870 and R01AI40882 (JHE). GSL was supported by a NIH Fellowship.

REFERENCES

1. Pedersen NC, Ho EW, Brown ML, Yamamoto JK. Isolation of T-lymphotropic virus from domestic cats with an immunodeficiency-like syndrome. *Science* 1987;235:790–793.
2. Pedersen NC. The Feline Immunodeficiency Virus. In: Levy, JA, editor. *The Retroviridae*. New York: Plenum Press; p 181–228.
3. Elder JH, Dean GA, Hoover EA, et al. Lessons from the cat: feline immunodeficiency virus as a tool to develop intervention strategies against human immunodeficiency virus type 1. *AIDS Res Hum Retroviruses* 1998;14:797–801.
4. Garry RF, Krieg AM, Cheevers WP et al. Retroviruses and their roles in chronic inflammatory diseases and autoimmunity. Levy, JA, editor. *The Retroviridae*. New York: Plenum Press; p 491–603.
5. Vandamme A-M, Van Vaerenbergh K, De Clercq E. Anti-human immunodeficiency virus drug combination strategies. *Antivir Chem Chemother* 1998;9:187–203.
6. Bendinelli M, Pistello M, Lombardi S et al. Feline immunodeficiency virus: an interesting model for AIDS studies and an important cat pathogen. *Clin Microbiol Rev* 1995;8:87–112.
7. Bennett M, Hart CA. Feline immunodeficiency virus infection—a model for HIV and AIDS? *J Med Microbiol* 1998;42:233–236.
8. Elder JH, Phillips TR. Feline immunodeficiency virus as a model for development of molecular approaches to intervention strategies against lentivirus infections. *Adv Virus Res* 1995;45:225–247.
9. McCune JM. Animal models of HIV-1 disease. *Science* 1997;278:2141–2142.
10. Willett BJ, Flynn JN, Hosie MJ. FIV infection of the domestic cat: an animal model for AIDS. *Immunol Today* 1997;18:182–189.
11. Deeks SG, Volberding PA. HIV-1 protease inhibitors. *AIDS Clin Rev* 1997;9:145–185.
12. Olson AJ, Goodsell DS. Automated docking and the search for HIV protease inhibitors. *SAR QSAR Environ Res* 1998;8:273–285.
13. Wlodawer A, Vondrasek J. Inhibitors of HIV-1 protease: A major success of structure-assisted drug design. *Annu Rev Biophys Biomol Struct* 1998;27:249–284.
14. Erickson JW. The not-so-great escape. *Nat Struct Biol* 1995;2:523–529.
15. Ribeiro RM, Bonhoeffer S, Nowak MA. The frequency of resistant mutant virus before antiviral therapy. *AIDS* 1998;12:461–465.
16. Kaplan AH. Constraints on the sequence diversity of the protease of human immunodeficiency virus type 1: a guide for drug design. *AIDS Res Hum Retroviruses* 1996;12:849–853.
17. Condra JH, Schleif WA, Blahy OM et al. In vivo emergence of HIV-1 variants resistant to multiple protease inhibitors. *Nature* 1995;374:569–571.
18. Erickson JW, Burt SK. Structural mechanisms of HIV drug resistance. *Annu Rev Pharmacol Toxicol* 1996;36:545–571.
19. Schinazi RF, Larder BA, Mellors JW. Mutations in retroviral genes associated with drug resistance. *Intl Antiviral News* 1997; 5,129–142.
20. Roberts NA, Craig JC, Sheldon J. Resistance and cross-resistance with saquinavir and other HIV protease inhibitors: Theory and practice. *AIDS* 1998;12:453–460.

21. Wlodawer A, Gustchina A, Reshetnikova L et al. Structure of an inhibitor complex of the proteinase from feline immunodeficiency virus. *Nat Struct Biol* 1995;2:480–488.
22. Gustchina A, Kervinen J, Powell DJ, Zdanov A, Kay J, Wlodawer A. Structure of equine infectious anemia virus proteinase complexed with an inhibitor. *Protein Sci* 1996;5:1453–1465.
23. Slee DH, Laslo KL, Elder JH et al. Selectivity in the inhibition of HIV and FIV protease: Inhibitory and mechanistic studies of pyrrolidine-containing α -keto amide and hydroxyethylamine core structures. *J Am Chem Soc* 1995;117:11867–11878.
24. Kervinen J, Lubkowski J, Zdanov A et al. Toward a universal inhibitor of retroviral proteases: comparative analysis of the interactions of LP-130 complexed with proteases from HIV-1, FIV, and EIAV. *Protein Sci* 1998;7:2314–2323.
25. Lee T, Laco GS, Torbett BE, Fox HS, Lerner D, Elder JH, Wong C-H. Analysis of the S3 and S3' subsite specificities of feline immunodeficiency virus (FIV) protease: development of a broad-based protease inhibitor efficacious against FIV, SIV, and HIV in vitro and ex vivo. *Proc Natl Acad Sci USA* 1998;95:939–944.
26. Talbott RL, Sparger EE, Lovelace KM et al. Nucleotide sequence and genomic organization of feline immunodeficiency virus. *Proc Natl Acad Sci USA* 1989;86:5743–5747.
27. Ratner L, Fisher A, Jagodzinski LL et al. Complete nucleotide sequences of functional clones of the AIDS virus. *AIDS Res Hum Retroviruses* 1987;3:57–69.
28. Gulnik SV, Suvorov LI, Liu B et al. Kinetic characterization and cross-resistance patterns of HIV-1 protease mutants selected under drug pressure. *Biochemistry* 1995;34:9282–9287.
29. Ratner L, Haseltine W, Patarca R et al. Complete nucleotide sequence of the AIDS virus, HTLV-III. *Nature* 1985;313:277–284.
30. Otwinowski Z, Minor W. Processing of X-ray diffraction data collected in oscillation mode. *Methods Enzymol* 1997;276:307–326.
31. Brünger A. X-PLOR version 3.1: A System for X-ray crystallography and NMR. New Haven, CT: Yale University Press; 1992.
32. Sheldrick GM, Schneider TR. SHELXL: High-resolution refinement. *Meth Enzymol* 1997;277:319–343.
33. Brünger AT. The free R value: a novel statistical quantity for assessing the accuracy of crystal structures. *Nature* 1992;355:472–474.
34. Jones TA, Kieldgaard M. Electron-density map interpretation. *Methods Enzymol* 1997;277:173–208.
35. Laskowski RA, MacArthur MW, Moss DS, Thornton JM. PROCHECK: A program to check the stereochemical quality of protein structures. *J Appl Crystallogr* 1993;26:283–291.
36. Lutz M. Programming Python. Sebastopol, CA: O'Reilly & Associates; 1996.
37. Python Language Website, <http://www.python.org/>.
38. InsightII 97.0 edition, San Diego, CA: Biosym Technologies; 1998.
39. Schechter I, Berger A. On the size of the active site in proteases. I. Papain. *Biochem Biophys Res Commun* 1967;27:157–162.
40. Jaskolski M, Tomasselli AG, Sawyer TK et al. Structure at 2.5 Å resolution of chemically synthesized human immunodeficiency virus type 1 protease complexed with a hydroxyethylene-based inhibitor. *Biochemistry* 1991;30:1600–1609.
41. Schnolzer M, Rackwitz HR, Gustchina A et al. Comparative properties of feline immunodeficiency virus (FIV) and human immunodeficiency virus type 1 (HIV-1) proteinases prepared by total chemical synthesis. *Virology* 1996;224:268–275.
42. Jadhav PK, Ala P, Woerner FJ et al. Cyclic urea amides: HIV-1 protease inhibitors with low nanomolar potency against both wild type and protease inhibitor resistant mutants of HIV. *J Med Chem* 1997;40:181–191.